

# Stable Single-Crystalline Body Centered Cubic Fe Nanoparticles

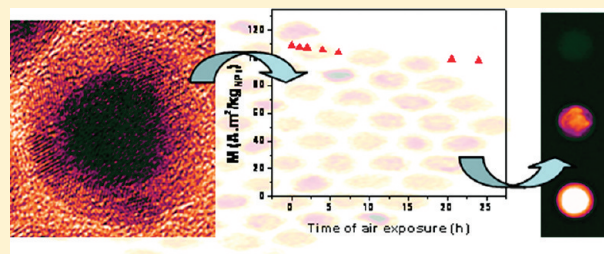
Lise-Marie Lacroix,<sup>†,§</sup> Natalie Frey Huls,<sup>‡</sup> Don Ho,<sup>†</sup> Xiaolian Sun,<sup>†</sup> Kai Cheng,<sup>†</sup> and Shouheng Sun<sup>\*,†</sup>

<sup>†</sup>Department of Chemistry, Brown University, Providence, Rhode Island 02912, United States

<sup>‡</sup>National Institute of Standards and Technology, Gaithersburg, Maryland 20899, United States

**§ Supporting Information**

**ABSTRACT:** We report a facile synthesis of body centered cubic (bcc) Fe nanoparticles (NPs) via the thermal decomposition of iron pentacarbonyl,  $\text{Fe}(\text{CO})_5$ , in the presence of hexadecylammonium chloride. These bcc-Fe NPs exhibit a drastically increased stability and magnetic moment ( $M_s = 164 \text{ A} \cdot \text{m}^2 \cdot \text{kg}^{-1} \text{ Fe}$ ) even in physiological solutions, and have much enhanced magnetic imaging contrast ( $r_2 = 220 \text{ s}^{-1} \cdot \text{mM}^{-1}$ ) and heating (SAR = 140 W · g<sup>-1</sup> Fe) effects. They may serve as robust probes for imaging and therapeutic applications.



**KEYWORDS:** Magnetic nanoparticles, bcc-Fe, nanoparticle stability, magnetic imaging, magnetic hyperthermia

Synthesis of stable magnetic nanoparticles (NPs) with high magnetization values has been a long-sought goal in developing NP probes for ultrasensitive biomedical imaging,<sup>1,2</sup> sensing,<sup>3,4</sup> and therapeutic applications.<sup>5,6</sup> Such NPs are also the essential building blocks for fabricating exchange-coupled nanocomposite magnets that are capable of storing high-density magnetic energy.<sup>7</sup> Among all NPs studied thus far, metallic Fe NPs have been the focus due to their high magnetization values and the ease with which their magnetization direction can be reversed. However, making monodisperse Fe NPs stable in ambient and biological environments has been extremely challenging. Here we report a facile synthesis of body centered cubic (bcc) Fe NPs via the decomposition of iron pentacarbonyl,  $\text{Fe}(\text{CO})_5$ , in the presence of hexadecylammonium chloride. These bcc-Fe NPs exhibit a drastically increased stability and magnetic moment even in physiological solutions. They show much enhanced effects on magnetic resonance imaging properties and magnetic heating. The reported synthesis represents an exciting advance in the synthesis of stable high moment Fe NPs for biomedical and other magnetic applications.

Conventionally, the high moment metallic NPs are made by thermal decomposition<sup>8,9</sup> and reduction<sup>10,11</sup> of metal precursors followed by high temperature<sup>12</sup> or other chemical treatments to form a robust shell of carbon,<sup>13</sup> oxides,<sup>14,15</sup> or noble metals.<sup>16</sup> We recently observed that a crystalline iron oxide shell obtained by a controlled oxidation of amorphous Fe (amor-Fe) NPs could protect the amor-Fe core from fast oxidation.<sup>14</sup> However, these core/shell  $\text{Fe}/\text{Fe}_3\text{O}_4$  NPs exhibit a relatively low magnetization value ( $90.6 \text{ A} \cdot \text{m}^2 \cdot \text{kg}^{-1} \text{ Fe}$ ). Highly crystalline Fe NPs could be made by reduction of a dimeric iron precursor with  $\text{H}_2$ .<sup>11,17</sup> These NPs have a magnetization close to the bulk value but are quickly oxidized once exposed to air. In our new synthesis, bcc-Fe NPs were obtained by thermal decomposition of  $\text{Fe}(\text{CO})_5$  in the presence of oleylamine, oleic acid, and hexadecylammonium chloride. When exposed to ambient environments, the surface layers of the bcc-Fe were oxidized into crystalline  $\text{Fe}_3\text{O}_4$ . These

new all crystalline bcc-Fe/ $\text{Fe}_3\text{O}_4$  NPs show much improved stability over any of the Fe-based NPs reported previously.

**Synthesis of bcc-Fe NPs.** In a four-neck flask, a mixture of 1-octadecene (ODE, 20 mL) and oleylamine (OAm) (0.3 mL, 1 mmol) and hexadecylammonium chloride (HDA·HCl, prepared according to Soulantica et al.<sup>18</sup> Supporting Information, 1 mmol) was stirred magnetically and degassed under  $\text{N}_2$  flow. The solution was heated to 120 °C and kept at this temperature for 30 min before it was heated further to 180 °C. Then under a  $\text{N}_2$  blanket,  $\text{Fe}(\text{CO})_5$  (0.7 mL, 5 mmol) was added and the reaction mixture was kept at 180 °C for 30 min. A color change from orange to brown and black was observed after ca. 20 min, indicating the decomposition of  $\text{Fe}(\text{CO})_5$  and the formation of Fe NPs. The solution was cooled down to 160 °C, and oleic acid (0.3 mL, 1 mmol) was added. The resultant solution was aged at 160 °C for another 30 min before it was cooled down to room temperature with NP flocculating and depositing around the magnetic bar. The supernatant was decanted, and the NP aggregate was washed with hexane and ethanol. The synthesis gave a black product with a 90% yield (based on Fe).

**Synthesis of OAm–PEG Surfactant.** To a solution of  $\alpha$ ,  $\omega$ -bis(2-carboxyethyl)poly(ethylene glycol) (PEG) ( $M_w = 600$ , 6.0 g, 10 mmol) and oleylamine (OAm) (2.675 g, 10 mmol) in 50 mL of dichloromethane (DCM) was added 122 mg of 4-(dimethylamino)pyridine (1 mmol) at room temperature under  $\text{N}_2$ . After being stirred for 10 min, the solution was cooled in an ice bath, and  $N,N'$ -dicyclohexylcarbodiimide (2.06 g, 10 mmol) in 10 mL of DCM was added dropwise into the solution over 1 h. The reaction mixture was allowed to reach room temperature and stirred for 24 h. The precipitation was removed by filtration, and the solvent was evaporated under reduced pressure to give light-yellow oil. The crude product was purified by washing it with cold ethyl ether twice and

**Received:** January 11, 2011

**Revised:** February 21, 2011

**Published:** March 18, 2011

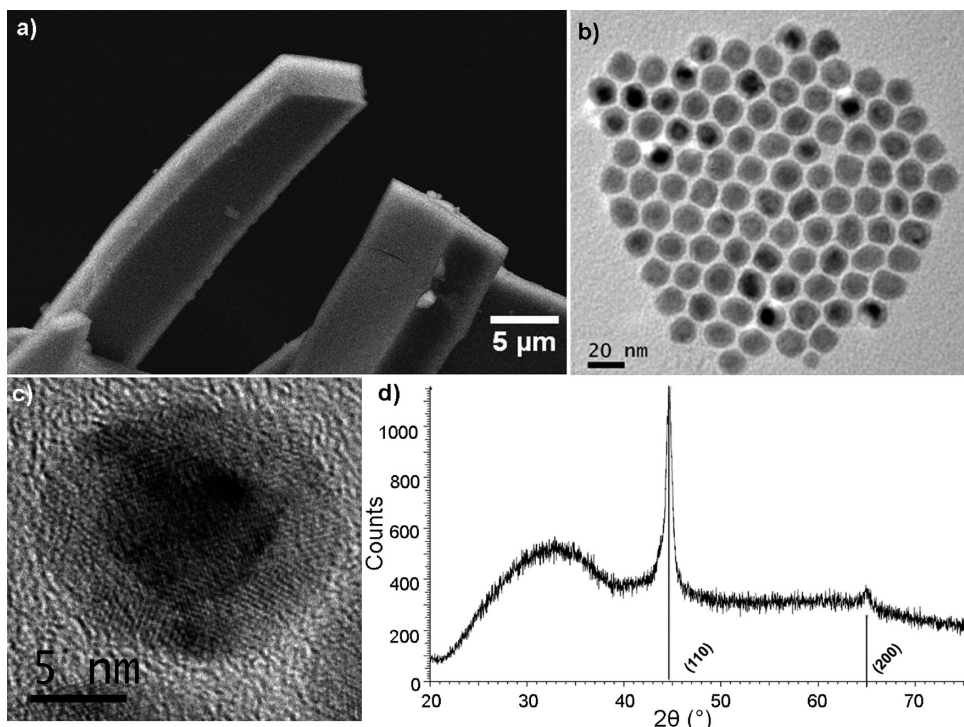


**Figure 1.** Morphological and structural characterization of bcc-Fe/Fe<sub>3</sub>O<sub>4</sub> NPs. (a) SEM image of the platelike Fe NP assembly obtained directly from the synthesis solution. (b) TEM image of the 15 nm NPs obtained from the redispersion of the plate assembly in hexanes. (c) HRTEM image of a single NP revealing the metallic bcc-Fe core and Fe<sub>3</sub>O<sub>4</sub> shell with Fe (110) and Fe<sub>3</sub>O<sub>4</sub> (222) planes indicated. (d) XRD pattern of the bcc-Fe NPs.

then dissolved in 10 mL of water with a brief sonication. The insoluble product was filtered off and the resultant solvent was lyophilized to get the desired product (yield 62%). The final compound was characterized by <sup>1</sup>H nuclear magnetic resonance (NMR) spectroscopy and matrix-assisted laser desorption/ionization (MALDI) mass spectrometry (MS).

**NP Surface Modification.** Fe/Fe<sub>3</sub>O<sub>4</sub> NPs (10 mg) were dried and dispersed in 1 mL of chloroform. A solution of OAm–PEG (50 mg) in 1 mL of chloroform was added to this solution that was further shaken mechanically for 1 h. The solvent was evaporated under a N<sub>2</sub> flow, and NPs were redispersed in deionized (DI) water (18.2 MΩ·cm) or PBS buffer. The excess surfactant was removed by dialysis tubings (MWCO:100000) in DI water for 24 h at room temperature, and any agglomerated NPs were removed by a Millex 0.22 μm syringe filter.

Figure 1a shows the scanning electron microscopy (SEM) image of representative aggregates of Fe NPs. It contains micrometer-long plates that consist of self-assembled Fe NPs. It indicates that in current synthetic conditions, the Fe NPs flocculate into plate-structure due likely to their lack of dispersibility in ODE and interactions with the magnetic bar. Once sonicated for 1 min, these plates could be redispersed in hexanes in the presence of OAm. A transmission electron microscopy (TEM) image (Figure 1b) shows that the dispersion contains 15 nm Fe NPs exhibiting a core/shell structure with a mean core diameter of 10.5 nm and a shell thickness at 2.5 nm.

A high-resolution TEM (HRTEM) image of a single Fe NP, slightly smaller than the mean size, clearly attests to the core/shell structure (Figure 1c). The core has a lattice fringe of 0.20 nm that is characteristic of the (110) planes of bcc-Fe. The shell is composed of several crystalline domains with a lattice fringe of 0.24 nm appearing in each domain. These fringes are from (222) planes of

the inverse spinel structured iron oxide. Although the exact nature of the oxide, Fe<sub>3</sub>O<sub>4</sub> or γ-Fe<sub>2</sub>O<sub>3</sub>, cannot be determined at this point, our early study shows that after Fe oxidation the majority of the phase is Fe<sub>3</sub>O<sub>4</sub>.<sup>19</sup>

To confirm the crystal structure of the as-synthesized NPs, X-ray diffraction (XRD) studies were performed on NP powder obtained either from the precipitated plates or after the solvent evaporation of the dispersed NPs. In both powder states, (110) and (200) peaks corresponding to the bcc-Fe are observed (Figure 1d) and no Fe<sub>3</sub>O<sub>4</sub> peaks can be seen due to the peak broadening of their small crystal domains.<sup>14</sup> A crystallite core size of 10 nm could be extracted from the half-width of the diffraction peaks using Scherrer's formula. Such a size is in good agreement with the mean core size of 10.5 nm determined from TEM analysis (Figure 1b and Figure S1, Supporting Information). As a comparison, Fe NPs synthesized via thermal decomposition of Fe(CO)<sub>5</sub> in the absence of HDA·HCl show no obvious diffraction pattern (Figure S2, Supporting Information). The difference in the diffraction patterns of the two kinds of Fe NPs prepared under very similar reaction conditions emphasizes the key role played by the HDA·HCl in the growth of crystalline Fe. Our experiments indicate that HDA·HCl slows down the decomposition of Fe(CO)<sub>5</sub>, facilitating the formation of a crystalline structure. This was seen by the color change of the reaction solution once the HDA·HCl was introduced. Without HDA·HCl, the characteristic orange color of Fe(CO)<sub>5</sub> disappeared 2 min after its addition at 180 °C, revealing a fast decomposition process. However, in the presence of HDA·HCl, the color of Fe(CO)<sub>5</sub> did not fade until 20 min later.

Field- and temperature-dependent magnetic measurements were performed on the dried crystalline bcc-Fe/Fe<sub>3</sub>O<sub>4</sub> powder using a superconducting quantum interference device (SQUID) magnetometer. At room temperature, these NPs are ferromagnetic and

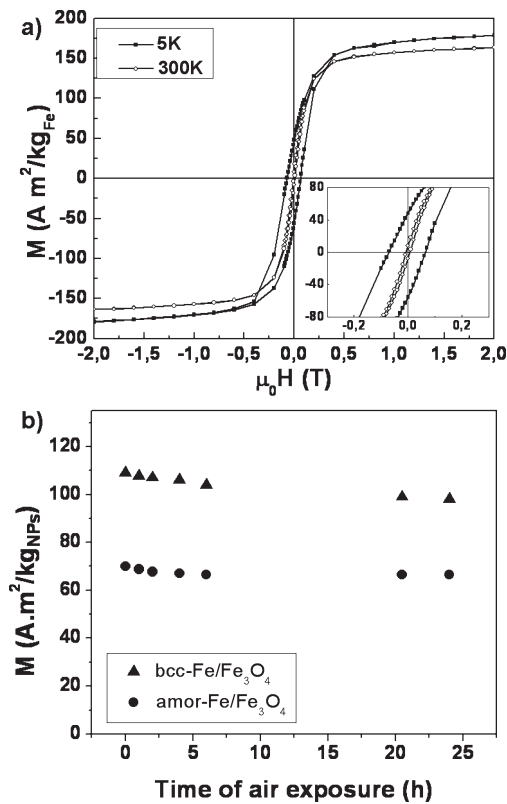


**Figure 2.** Magnetic characterization of the Fe/Fe<sub>3</sub>O<sub>4</sub> NPs. (a) Magnetic hysteresis loops of the bcc-Fe/Fe<sub>3</sub>O<sub>4</sub> NPs recorded at 5 K (solid cubes) and 300 K (open circles). Inset: a close look of the hysteresis loops between −0.3 and 0.3 T. (b) The change of the magnetization values as a function of air exposure time of the bcc-Fe/Fe<sub>3</sub>O<sub>4</sub> and the amor-Fe/Fe<sub>3</sub>O<sub>4</sub> NPs of similar size at 1.5 T and room temperature.

exhibit a high magnetization at 2 T with a saturation magnetization value  $M_s = 164 \text{ A} \cdot \text{m}^2 \cdot \text{kg}^{-1} \text{Fe}$  and coercive field  $H_c = 14 \text{ mT}$  (Figure 2a). Once the temperature is cooled down to 5 K, their  $M_s$  and  $H_c$  increase up to  $180 \text{ A} \cdot \text{m}^2 \cdot \text{kg}^{-1} \text{Fe}$  and 80 mT (Figure 2a and Figure S3a, Supporting Information). The room temperature ferromagnetic behavior of these NPs was further attested by the temperature-dependent zero-field cooling (ZFC) and field cooling (FC) measurement (Figure S3b, Supporting Information). From the ZFC–FC curve, we see no sign of superparamagnetic transition up to 350 K, which indicates that our NPs exhibit a relatively large anisotropy. The increase in anisotropy is attributed to the magnetic coupling between the core and the shell and the details of the magnetic studies on these core/shell NPs will be published separately. The difference in magnetization between our NPs and the bulk Fe ( $220 \text{ A} \cdot \text{m}^2 \cdot \text{kg}^{-1} \text{Fe}$ ) is due to the presence of the ferrimagnetic iron oxide shell that has a lower magnetization value (bulk Fe<sub>3</sub>O<sub>4</sub>:  $95 \text{ A} \cdot \text{m}^2 \cdot \text{kg}^{-1} \text{Fe}$ ). From bulk magnetization values of Fe and Fe<sub>3</sub>O<sub>4</sub> as well as the core/shell Fe/Fe<sub>3</sub>O<sub>4</sub> NP diameter and magnetization data, we estimate that these core/shell NPs have a core ca. 10 nm in diameter and a shell of 2.1 nm thickness (eqs S4, Supporting Information), consistent with what we obtained from both the TEM and XRD analyses.

The air stability of these bcc-Fe/Fe<sub>3</sub>O<sub>4</sub> NPs in both hexane dispersion and powder form was investigated by a vibrating sample magnetometer (VSM). During the first 24 h of air exposure, hysteresis loops of the powder samples (in the case of MNP dispersion in hexane, hexane was evaporated to obtain the NP

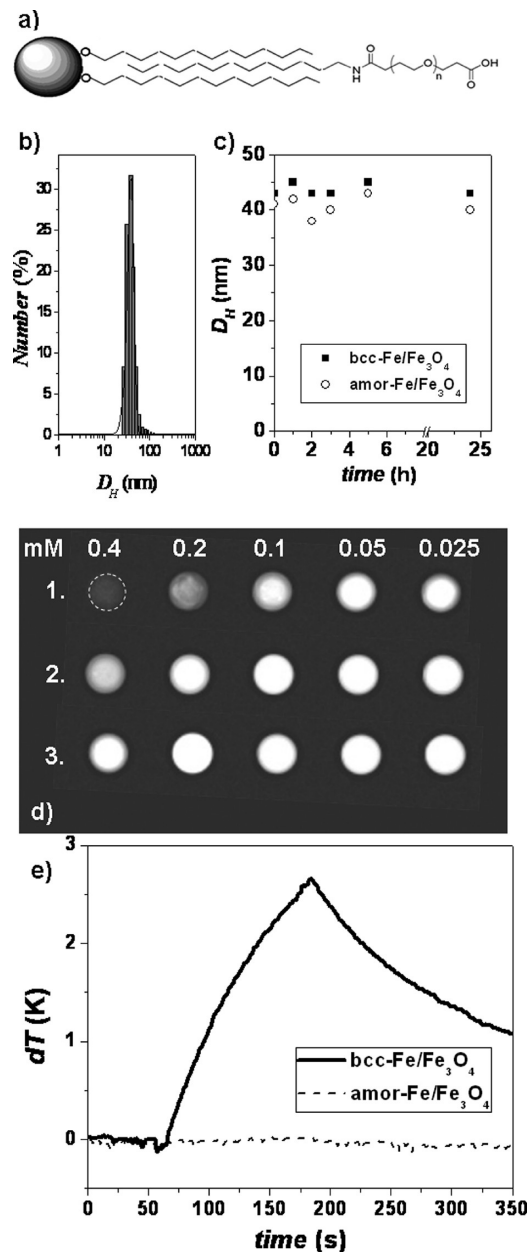


**Figure 3.** Modification of Fe/Fe<sub>3</sub>O<sub>4</sub> NPs for biomedical applications. (a) Schematic view of the double layer hydrophobic and hydrophilic coating around each NP. (b) Hydrodynamic diameters measured by dynamic light scattering (DLS) for the bcc-Fe/Fe<sub>3</sub>O<sub>4</sub> NPs and (c) hydrodynamic diameter change as a function of incubation time under physiological conditions. (d)  $T_2$ -weighted images of the bcc-Fe/Fe<sub>3</sub>O<sub>4</sub> NPs (1), amor-Fe/Fe<sub>3</sub>O<sub>4</sub> NPs (2), and 16 nm Fe<sub>3</sub>O<sub>4</sub> NPs (3). (e) Temperature profiles measured for the bcc-Fe/Fe<sub>3</sub>O<sub>4</sub> (solid line) and the amor-Fe/Fe<sub>3</sub>O<sub>4</sub> NPs (dashed line).

powder sample) were recorded frequently (Figure S5a, Supporting Information) and magnetization values at 1.5 T were extracted (Figure 2b). We can see that the crystalline Fe<sub>3</sub>O<sub>4</sub> protected Fe NPs show little magnetization change over 24 h. They are stable even after a month of air exposure period (Figure S5b, Supporting Information). For comparison, amor-Fe/Fe<sub>3</sub>O<sub>4</sub> NPs with 10 nm core and 2.5 nm shell were also synthesized through a seed-mediated growth followed by the controlled Me<sub>3</sub>NO oxidation (Supporting Information<sup>14</sup>) and studied. Their magnetization values are given in

**Table 1.** Relaxivities  $r_2$  at 3 T and 25 °C and Specific Absorption Rate (SAR) Measured at 170 kHz and 33 mT of Three Different Kinds of NPs with Sizes of 15–16 nm and Same Surface Functionalization<sup>a</sup>

NPs	$r_2$ ( $\text{s}^{-1} \cdot \text{mM}^{-1}$ )	SAR ( $\text{W} \cdot \text{g}^{-1}$ )
bcc-Fe/Fe <sub>3</sub> O <sub>4</sub>	220	140
amor-Fe/Fe <sub>3</sub> O <sub>4</sub>	67	10
Fe <sub>3</sub> O <sub>4</sub>	24	5
Ferridex	110 <sup>21</sup>	
14 nm FeCo		150 <sup>24</sup>

<sup>a</sup> The  $r_2$  values of the commercial Ferridex and FeCo nanoparticles are also included.

Figure 2b. From these two different kinds of Fe/Fe<sub>3</sub>O<sub>4</sub> NPs, we conclude that the bcc-Fe/Fe<sub>3</sub>O<sub>4</sub> NPs have the following benefits: (i) the Fe core is highly crystalline and the protective crystalline iron oxide shell is formed directly from the native oxidation of this bcc-Fe core; (ii) their net magnetization at 1.5 T ( $M_s = 102 \text{ A} \cdot \text{m}^2 / \text{kg}_{\text{MNPs}}$ ) is improved by a factor of 50% over the amor-Fe/Fe<sub>3</sub>O<sub>4</sub> NPs ( $M_s = 70 \text{ A} \cdot \text{m}^2 / \text{kg}_{\text{MNPs}}$ ); and (iii) they demonstrate a long-term stability and their magnetization dropped only about 20% to 82  $\text{A} \cdot \text{m}^2 / \text{kg}_{\text{MNPs}}$  after a month—this magnetization value is still far above those reported for Fe<sub>3</sub>O<sub>4</sub> NPs.

The as-synthesized NPs described above are coated with OAm and oleate and are hydrophobic. To make them compatible with biological media, an amphiphilic oleylamine–poly(ethylene glycol) (OAm-PEG) surfactant (Figure 3a and Supporting Information) was selected to modify the NP surface. Through the interlock of the hydrophobic chains between OAm/oleate and OAm-PEG, a stable hydrophobic/hydrophilic double-layer was formed on each NP. The OAm-PEG coated NPs were stable in phosphate-buffered saline (PBS) (pH = 7) at 37 °C as evidenced by their unchanged hydrodynamic sizes in the 24 h incubation period (Figure 3b,c).

The water-soluble bcc-Fe/Fe<sub>3</sub>O<sub>4</sub> NPs can serve as excellent probes for both magnetic resonance imaging (MRI) and magnetic heating. In MRI, magnetic NPs show stronger contrast effect on the spin–spin relaxation ( $T_2$ ) process and the related relaxivity ( $r_2$ ) is dependent upon  $M_s^2$  and  $d^{-6}$  with  $d$  being the distance between the magnetic core and the surrounding protons.<sup>20</sup> The effectiveness of our bcc-Fe/Fe<sub>3</sub>O<sub>4</sub> NPs as contrast agents was compared to the amor-Fe/Fe<sub>3</sub>O<sub>4</sub> NPs and Fe<sub>3</sub>O<sub>4</sub> NPs of similar sizes and same OAm-PEG functionalization. As expected from the magnetization study, the bcc-Fe/Fe<sub>3</sub>O<sub>4</sub> NPs have the best darkening effect among three different types of NPs (Figure 3d). Their respective relaxivity coefficients ( $r_2$ ), summarized in Table 1, are extracted from the slope of the  $1/T_2$  curves vs the Fe molarity (Figure S6, Supporting Information). Even though these NPs are all surrounded by a relatively thick coating (15 nm), the bcc-Fe/Fe<sub>3</sub>O<sub>4</sub> NPs still exhibit a  $r_2 = 220 \text{ s}^{-1} \cdot \text{mM}^{-1}$ , better than the typical iron oxide NP contrast agent Feridex ( $110 \text{ s}^{-1} \cdot \text{mM}^{-1}$ )<sup>21</sup> and comparable with the optimized ferrite NPs with 2 nm thick coating.<sup>22</sup> On the basis of the  $r_2$  relationship with  $d^{-6}$ , we estimate that these bcc-Fe/Fe<sub>3</sub>O<sub>4</sub> NPs could have an order of magnitude increase in relaxivity if their coating thickness is reduced by only 5 nm.

The stable weakly ferromagnetic bcc-Fe/Fe<sub>3</sub>O<sub>4</sub> NPs with high magnetic moment should also be efficient heaters for magnetic fluid hyperthermia (MFH) applications.<sup>23–25</sup> The cancer treatment by hyperthermia, based on the sensitivity of cancer cells to heat, has been explored extensively with NPs playing the key role as the local

heaters.<sup>6</sup> Under an alternating magnetic field, the magnetization direction of NPs can be rotated via Brownian and Néel processes, generating heat.<sup>26</sup> The NP heating efficiency can be quantified by the specific absorption rate (SAR):  $\text{SAR} (\text{W} \cdot \text{g}^{-1}) = A \cdot f$  with  $A$  being the area of the hysteresis loop and  $f$  the frequency of the external magnetic field applied. To assess the heating efficiencies of the bcc-Fe/Fe<sub>3</sub>O<sub>4</sub>, amor-Fe/Fe<sub>3</sub>O<sub>4</sub>, and Fe<sub>3</sub>O<sub>4</sub> NPs of similar sizes, we dispersed these NPs in water and applied an alternating magnetic field with  $f = 177 \text{ kHz}$  and  $\mu_0 H_{\text{max}} = 33 \text{ mT}$ , fulfilling the physiological limitations  $H_{\text{max}} \cdot f < 5 \times 10^9 \text{ A} \cdot \text{m}^{-1} \cdot \text{s}^{-1}$ , and  $f > 50 \text{ kHz}$ .<sup>28</sup> The heating profiles of the bcc- and amor-Fe/Fe<sub>3</sub>O<sub>4</sub> NPs are given in Figure 3e. The SARs for all three kinds of NPs are determined from the initial increase of their heating profiles<sup>6</sup> and summarized in Table 1. Due to their higher magnetization value and small coercive field, the bcc-Fe/Fe<sub>3</sub>O<sub>4</sub> NPs with a SAR value of  $140 \text{ W} \cdot \text{g}^{-1}$  are much more efficient heaters than both the amor-Fe/Fe<sub>3</sub>O<sub>4</sub> and Fe<sub>3</sub>O<sub>4</sub> NPs. This  $140 \text{ W} \cdot \text{g}^{-1}$  value is one of the highest reported thus far under similar conditions, comparable with the ferromagnetic 14 nm FeCo NPs<sup>24</sup> and two times higher than the best results reported for 20 nm iron oxide NPs.<sup>29</sup> The heating efficiency of the bcc-Fe/Fe<sub>3</sub>O<sub>4</sub> NPs could be further improved if these NPs could be fully saturated—under the magnetic field applied (33 mT), they show minor hysteresis behavior (Figure S7, Supporting Information) and their minor loop losses are evidenced by the typical time-dependent temperature increase over the applied field (11 to 33 mT) and linear  $H^2$ -SAR relationship (Figure S8, Supporting Information).<sup>27</sup> Tuning the size and coating thickness of these bcc-Fe/Fe<sub>3</sub>O<sub>4</sub> NPs is the next step to achieve full magnetization under the 33 mT field and the optimum heating efficiency.

We have reported a facile synthesis of highly crystalline Fe/Fe<sub>3</sub>O<sub>4</sub> NPs from the thermal decomposition of Fe(CO)<sub>5</sub>. Different from all previous Fe(CO)<sub>5</sub>-based syntheses where amorphous Fe NPs are always obtained, by adding an alkyl ammonium chloride salt, our current approach leads to single crystalline 15 nm bcc-Fe NPs. Once exposed to air, these 15 nm NPs are only partially oxidized and the resultant core/shell bcc-Fe/Fe<sub>3</sub>O<sub>4</sub> NPs with a 10 nm bcc-Fe core are stable in air and have a high magnetization value ( $164 \text{ A} \cdot \text{m}^2 \cdot \text{kg}^{-1}$ ). These core/shell NPs can be functionalized with oleylamine–PEG surfactant and dispersed in water or PBS without showing obvious sign of deep oxidation in the testing periods up to a month. They have much enhanced contrast and heating effects and should serve as robust probes for simultaneous magnetic resonance imaging and magnetic fluid hyperthermia applications.

## ■ ASSOCIATED CONTENT

**S Supporting Information.** (1) Experimental procedure (general synthesis, HDA·HCl preparation, NP characterization, MRI, and MFH experiments), (2) size distribution, (3) XRD pattern of amor-Fe/Fe<sub>3</sub>O<sub>4</sub> NPs, (4) magnetic characterization of bcc-Fe/Fe<sub>3</sub>O<sub>4</sub> NPs (ZFC/FC; Ms(T)); (5) details of the magnetic core size calculation, (6) magnetic characterization of air-exposed NPs (M(H); M(T)), (7) MRI transverse relaxation signals, (8) minor-loop M(H) of bcc-Fe/Fe<sub>3</sub>O<sub>4</sub> NPs, (9) MFH T(t) curve, SAR evolution as a function of the applied field. This material is available free of charge via the Internet at <http://pubs.acs.org>.

## ■ AUTHOR INFORMATION

### Corresponding Author

\*E-mail: ssun@brown.edu.

**Present Addresses**

<sup>§</sup>Present address: Université de Toulouse, INSA, UPS, LPCNO (Laboratoire de Physique et Chimie des Nano-Objets), F-31077 Toulouse, France.

**ACKNOWLEDGMENT**

Supported in part by NIH/NCI 1R21CA12859, DOE/EPS-CoR DE-FG02-07ER36374, DARPA/ARO W911NF-08-1-0249, and the Brown Imaging Fund. The authors thank J. Orchado for help with ICP measurements. L.-M.L. thanks the French State/D4S grant for supporting her work at Brown University. N.F.H. thanks C. L. Dennis of NIST for experimental help and useful comments.

**REFERENCES**

- (1) Bouchard, L.-S.; Anwar, M. S.; Liu, G. L.; Hann, B.; Xie, Z. H.; Gray, J. W.; Wang, X.; Pines, A.; Chen, F. F. *Proc. Natl. Acad. Sci. U.S.A.* **2009**, *106*, 4085–4089.
- (2) Lin, W.; Hyeon, T.; Lanza, G. M.; Zhang, M.; Meade, T. J. *MRS Bull.* **2009**, *34*, 441–448.
- (3) Li, Y.; Srinivasan, B.; Jing, Y.; Yao, X.; Hugger, M. A.; Wang, J.-P.; Xing, C. *J. Am. Chem. Soc.* **2010**, *132*, 4388–4392.
- (4) Haun, J. B.; Yoon, T.-J.; Lee, H.; Weissleder, R. *Wiley Interdiscip. Rev.: Nanomed. Nanobiotechnol.* **2010**, *2*, 291–304.
- (5) Shubayev, V. I.; Pisanic, T. R.; Jin, S. H. *Adv. Drug Delivery Rev.* **2009**, *61*, 467–477.
- (6) Lacroix, L.-M.; Ho, D.; Sun, S. *Curr. Top. Med. Chem.* **2010**, *10*, 1184–1197.
- (7) Zeng, H.; Li, J.; Liu, J. P.; Wang, Z. L.; Sun, S. *Nature* **2002**, *420*, 395–398.
- (8) Farrell, D.; Majetich, S. A.; Wilcoxon, J. P. *J. Phys. Chem. B* **2003**, *107*, 11022–11030.
- (9) Shavel, A.; Rodríguez-González, B.; Spasova, M.; Farle, M.; Liz-Marzán, L. M. *Synthesis. Adv. Funct. Mater.* **2007**, *17*, 3870–3876.
- (10) Dumestre, F.; Chaudret, B.; Amiens, C.; Renaud, P.; Fejes, P. *Science* **2004**, *303*, 821–823.
- (11) Lacroix, L.-M.; Lachaize, S.; Falqui, A.; Respaud, M.; Chaudret, B. *J. Am. Chem. Soc.* **2009**, *131*, 549–557.
- (12) Sun, S.; Zeng, H. *J. Am. Chem. Soc.* **2002**, *124*, 8204–8205.
- (13) Desvaux, C.; Amiens, C.; Fejes, P.; Renaud, P.; Respaud, M.; Lecante, P.; Snoeck, E.; Chaudret, B. *Nat. Mater.* **2005**, *4*, 750–753.
- (14) Peng, S.; Wang, C.; Xie, J.; Sun, S. *J. Am. Chem. Soc.* **2006**, *128*, 10676–10677.
- (15) Bönnemann, H.; Brand, R. A.; Brijoux, W.; Hofstadt, H.-W.; Frerichs, M.; Kempfer, V.; Maus-Friedrichs, W.; Matoussevitch, N.; Nagabhushana, K. S.; Voigts, F.; Caps, V. *Appl. Organomet. Chem.* **2005**, *19*, 790–796.
- (16) Lee, W.-R.; Kim, M. G.; Choi, J.-R.; Park, J.-I.; Ko, S. J.; Oh, S. J.; Cheon, J. *J. Am. Chem. Soc.* **2005**, *127*, 16090–16097.
- (17) Snoeck, E.; Gatel, C.; Lacroix, L.-M.; Blon, T.; Lachaize, S.; Carrey, J.; Respaud, M.; Chaudret, B. *Nano Lett.* **2008**, *8*, 4293–4298.
- (18) Soulantica, K.; Maisonnat, A.; Fromen, M.-C.; Casanove, M.-J.; Chaudret, B. *Angew. Chem., Int. Ed.* **2003**, *42*, 1945–1947.
- (19) Yu, H.; Chen, M.; Rice, P. M.; Wang, S. X.; White, R. L.; Sun, S. *Nano Lett.* **2005**, *5*, 379–382.
- (20) Koenig, S. H.; Keller, K. E. *Magn. Reson. Med.* **1995**, *34*, 227–233.
- (21) Jang, J.-T.; Nah, H.; Lee, J.-H.; Moon, S. H.; Kim, M. G.; Cheon, J. *Angew. Chem., Int. Ed.* **2009**, *48*, 1234–1238.
- (22) Lee, J.-H.; Huh, Y.-M.; Jun, Y.-W.; Seo, J.-W.; Jang, J.-T.; Song, H.-T.; Kim, S.; Cho, E.-J.; Yoon, H.-G.; Suh, J.-S.; Cheon, J. *Nat. Med.* **2007**, *13* (1), 95–99.
- (23) Carrey, J.; Mehdaoui, B.; Respaud, M., *J. Appl. Phys.*, in press.
- (24) Lacroix, L.-M.; Bel Malaki, R.; Carrey, J.; Lachaize, S.; Respaud, M.; Goya, G. F.; Chaudret, B. *J. Appl. Phys.* **2009**, *105*, No. 023911.
- (25) Mehdaoui, B.; Meffre, A.; Lacroix, L.-M.; Carrey, J.; Lachaize, S.; Gougeon, M.; Respaud, M.; Chaudret, B. *J. Magn. Magn. Mater.* **2010**, *322*, L49.
- (26) Mornet, S.; Vasseur, S.; Grasset, F.; Duguet, E. *J. Mater. Chem.* **2004**, *14*, 2161–2175.
- (27) Hergt, R.; Dutz, S. *J. Magn. Magn. Mater.* **2007**, *311*, 187–192.
- (28) Jordan, A.; Scholz, R.; Wüst, P.; Fähling, H.; Felix, R. *J. Magn. Magn. Mater.* **1999**, *201*, 413–419.
- (29) Zhang, L.-Y.; Gu, H.-C.; Wang, X.-M. *J. Magn. Magn. Mater.* **2007**, *311*, 228–233.